A General, Efficient Method of Incorporation of Metal Ions into Ultrathin TiO_2 Films

Junhui He,[†] Izumi Ichinose,[†] Shigenori Fujikawa,[†] Toyoki Kunitake,*[,†] and Aiko Nakao[‡]

Frontier Research System (FRS) and Surface Characterization Division, The Institute of Physical and Chemical Research (RIKEN), Hirosawa 2-1, Wako-shi, Saitama, 351-0198 Japan

Received December 20, 2001. Revised Manuscript Received May 29, 2002

A general, efficient method was developed to incorporate a variety of second metal ions into ultrathin TiO_2 films. The thin films were first prepared by the surface sol−gel process from a mixture of the matrix-forming titanium alkoxide and template magnesium alkoxide. Mg^{2+} ion was removed by acid/base treatment, forming highly efficient and robust ion-exchange sites. A large variety of metal ions, including alkaline, alkaline earth, transition, and rare earth elements, were then incorporated into the thin films by ion exchange with Na^+. The amount of incorporation increased with increasing charge of the metal ions. The rate of the ion-exchange process was investigated in the case of Gd^{3+}. The incorporated metal ions were immobilized by thermal treatment at 450 °C. The UV absorption edge of the TiO_2 film was extended to the visible region by Fe^{3+} doping and calcination.

Introduction

The incorporation of second metal ions into metal-oxide matrixes is a very useful method for modifying physical and chemical properties of metal oxides to bring about new functional features. For example, TiO_2 doped with ions of transition metals,[1] aluminum,[2] and beryllium[3] was extensively studied as a photoanode in the photoelectrolysis of water. Much enhanced photocatalytic activity was observed for TiO_2 species highly dispersed in SiO_2[4] and for TiO_2 matrixes doped with iron(III)[5] and rare earth metal[6] ions. Rb^+-modified V_2O_5/SiO_2 could selectively convert 2-methylpropane to 2-methylpropane-2-ol by photoassisted oxidation.[7] In the preparation of thermal catalysts for redox reactions, metal oxides are often used as supports. Doping of TiO_2 with ions with different valencies but with sizes similar to Ti^{IV} improves the catalytic activity. For example, doping of anatase with Li^+, Nb^{5+}, and W^{6+} resulted in increased specific surface areas.[8] Highly dispersed Cu ion on TiO_2 or CeO_2 support was readily reduced and oxidized.[9,10] Whereas TiO_2-supported Cu showed catalytic activity for methanol reforming,[11] NO and N_2O decomposition,[12−14] combustion of soot particles, etc., Cu/CeO_2 revealed high catalytic activity for CO oxidation and SO_2 reduction.[15] More recently, highly dispersed CeO_2 on discrete barium hexaaluminate nanoparticles was reported to display excellent methane combustion activity.[16] On the other hand, Nb-doped mesoporous silicates have been used as supports of metalloporphyrins for enzyme-mimicking catalysis.[17] Further examples of metal ion incorporation include

* To whom correspondence should be addressed. Fax: +81-48-464-6391. E-mail: kunitake@ruby.ocn.ne.jp.

† Frontier Research System (FRS).

‡ Surface Characterization Division.

(1) (a) Matsumoto, Y.; Kurimoto, J.; Amagasaki, Y.; Sato, E. *J. Electrochem. Soc.* **1980**, *127*, 2148−2152. (b) Matsumoto, Y.; Kurimoto, J.; Shimizu, T.; Sato, E. *J. Electrochem. Soc.* **1981**, *128*, 1040−1044. (c) Augustynski, J.; Hinden, J.; Stalder, C. *J. Electrochem. Soc.* **1977**, *124*, 1063−1064. (d) Takahashi, Y.; Ogiso, A.; Tomoda, R.; Sugiyama, K.; Minoura, H.; Tsuiki, M. *J. Chem. Soc., Faraday Trans. 1* **1982**, *78*, 2563−2571. (e) Habazaki, H.; Takahiro, K.; Yamaguchi, S.; Shimizu, K.; Skeldon, P.; Thompson, G. E.; Wood, G. C. *Philos. Mag. A* **1998**, *78*, 171−187.

(2) Ghosh, A. K.; Maruska, H. P. *J. Electrochem. Soc.* **1977**, *124*, 1516−1522.

(3) Stalder, C.; Augustynski, J. *J. Electrochem. Soc.* **1979**, *126*, 2007−2011.

(4) Anpo, M.; Nakaya, H.; Kodama, S.; Kubokawa, Y.; Domen, K.; Onishi, T. *J. Phys. Chem.* **1986**, *90*, 1633−1636.

(5) Ohno, T.; Haga, D.; Fujihara, K.; Kaizaki, K.; Matsumura, M. *J. Phys. Chem. B* **1997**, *101*, 6415−6419.

(6) Shuji, M.; Keiji, Y.; Sumio, N.; Taku, M.; Hisanobu, W. In *Proceedings of the 79th CSJ National Meeting*; Chemical Society of Japan: Tokyo, Japan, 2001; p 436.

(7) Tanaka, T.; Takenaka, S.; Funabiki, T.; Yoshida, S. *J. Chem. Soc., Faraday Trans.* **1996**, *92*, 1975−1979.

(8) Tsevis, A.; Spanos, N.; Koutsoukos, P. G.; A. J. v. d. Linde, Lyklema, J. *J. Chem. Soc., Faraday Trans.* **1998**, *94*, 295−300.

(9) Nagashima, K.; Kokusen, H.; Ueno, N.; Matsuyoshi, A.; Kosaka, T.; Hasegawa, M.; Hoshi, T.; Ebitani, K.; Kaneda, K.; Aritani, H.; Hasegawa, S. *Chem. Lett.* **2000**, 264−265.

(10) Tschöpe, A.; Trudeau, M. L.; Ying, J. Y. *J. Phys. Chem. B* **1999**, *103*, 8858−8863.

(11) Kobayashi, H.; Takezawa, N.; Minochi, C. *J. Catal.* **1981**, *69*, 487−494.

(12) Boccuzzi, F.; Guglielminotti, E.; Martra, G.; Cerrato, G. *J. Catal.* **1994**, *146*, 449−459.

(13) Aritani, H.; Akasaka, N.; Tanaka, T.; Funabiki, T.; Yoshida, S.; Gotoh, H.; Okamoto, Y. *J. Chem. Soc., Farady Trans.* **1996**, *92*, 2625−2630.

(14) Aritani, H.; Tanaka, T.; Funabiki, T.; Yoshida, S.; Gotoh, H.; Okamoto, Y. *J. Catal.* **1997**, *168*, 412−420.

(15) (a) Liu, W.; Flytzani-Stephanopoulos, M. *J. Catal.* **1995**, *153*, 304−316. (b) Tschöpe, A.; Liu, W.; Flytzani-Stephanopoulos, M.; Ying, J. Y. *J. Catal.* **1995**, *157*, 42−50. (c) Liu, W.; Flytzani-Stephanopoulos, M. In *Environmental Catalysis*; Armor, J. N., Ed.; ACS Symposium Series 552; American Chemical Society: Washington, DC, 1994; p 375. (d) Liu, W.; Sarofim, A. F.; Flytzani-Stephanopoulos, M. *Appl. Catal. B* **1994**, *4*, 167−186. (e) Tschöpe, A.; Ying, J. Y.; Liu, W.; Flytzani-Stephanopoulos, M. In *Materials and Processes for Environmental Protection*; Voss, K. E., Quick, L. M., Gadgil, P. N., Adkins, C. L. J., Eds.; MRS Symposium Proceedings 344; Materials Research Society: Pittsburgh, PA, 1994; p 133. (f) Tschöpe, A.; Schaadt, D.; Birringer, R.; Ying, J. Y. *Nanostruct. Mater.* **1997**, *9*, 423−432.

(16) Zarur, A. J.; Ying, J. Y. *Nature* **2000**, *403*, 65−67.

(17) Zhang, L.; Sun, T.; Ying, J. Y. *Chem. Commun.* **1999**, 1103−1104.

10.1021/cm010880w CCC: $22.00
Published on Web 07/12/2002

modification of film optical properties by sequential implantation of Sc (Ti), O, and Ag ions in silica[18] and the preparation of metal ion (Ca^{2+}, Zn^{2+})-doped cerium dioxide as UV filters.[19] Luminescent materials have been prepared by doping rare earth metal ions in silica matrixes.[20] Fukumura et al. predicted that ZnO would become ferromagnetic by doping with 3d transition elements,[21] and they recently succeeded in preparing Co-doped TiO_2 thin films that exhibited ferromagnetism even at room temperature.[22]

The approaches that have been used for the incorporation of metal ions into metal-oxide matrixes can be classified as follows: MOCVD, ion implantation, epitaxy, laser ablation, metal sputtering followed by anodic oxidation, calcination of mixed metal oxides, conventional coprecipitation, sol−gel processing, and impregnation. They naturally have specific advantages and disadvantages, and the general application to varied metal ions of each approach is not possible.

The surface sol−gel process is a newly developed technique by which ultrathin metal oxide films of controlled thickness can be fabricated.[23] We have shown that intricate structures of many organic compounds can be imprinted in the network of TiO_2 gel.[24,25] Our subsequent study demonstrated that Cu^{2+} and Zn^{2+} ions were effective as template species[26] with the help of ethylenediamine ligand. The use of metal oxide gel itself as imprinting sites for metal ions has been our long-standing target, because it is conceivable that oxygen bridges and free hydroxy groups act as ligands to metal ions. In the present study, we showed that it was in fact the case. The loosely bound Mg^{2+} ion in the TiO_2 gel matrix provided Mg^{2+}-templated sites after its removal by acid treatment. These sites underwent efficient ion exchange with a large variety of other metal ions.

Experimental Section

Materials. KNO_3, $LiNO_3$, $Ca(NO_3)_2 \cdot 4H_2O$, $Mg(NO_3)_2 \cdot 6H_2O$, $Ba(NO_3)_2$, $Fe(NO_3)_3 \cdot 9H_2O$, $Co(NO_3)_2 \cdot 6H_2O$, $AgNO_3$, $Cr(NO_3)_3 \cdot 9H_2O$, $Pd(NO_3)_2$, $Cd(NO_3)_2 \cdot 4H_2O$, $La(NO_3)_3 \cdot 6H_2O$, $Gd(NO_3)_3 \cdot 6H_2O$, 2-mercaptoethanol, aqueous HCl, and NaOH (1 M) were purchased from Kanto Chemical. $Mn(NO_3)_2 \cdot 6H_2O$ was purchased from Wako Pure Chem. Ti(O-*n*Bu)$_4$ was obtained from Gelest, Inc. All of these chemicals were guaranteed reagents and used as purchased. Ultrapure water with the specific resistance of 18.3 MΩ·cm was obtained by reversed osmosis followed by ion exchange and filtration (Yamato-WQ500, Millipore, Tokyo, Japan). Aqueous solutions of given pH's were prepared by adjusting the pH of ultrapure water with aqueous HCl or NaOH (1 M).

Quartz Crystal Microbalance. A quartz crystal microbalance (QCM, 9 MHz) device manufactured by USI System, Fukuaka, Japan, was used for monitoring layer-by-layer film assembly and removal of template and for evaluating the incorporation of various metal ions into resulting films. Gold-coated QCM resonators were treated with piranha solution (96.0% sulfuric acid/30.0−35.5% hydrogen peroxide, 3/1, v/v), rinsed with pure water, and dried by being flushed with nitrogen gas. Then, they were immersed in an ethanol solution of 2-mercaptoethanol (10 mM) for 12 h, followed by rinsing with ethanol and drying with nitrogen gas. Frequency shifts due to the surface sol−gel cycle and removal and incorporation of metal ions were monitored in air after drying and were transformed into mass changes by using the Sauerbrey equation.[27] In our system, a frequency decrease of 1 Hz corresponds to a mass increase of 0.87 ng. The thickness (d) of an adsorbed film on one side of a resonator is given by[23]

$$2d\ (\text{Å}) = -\frac{\Delta F\ (\text{Hz})}{1.832\rho\ (\text{g/cm}^3)} \qquad (1)$$

where ρ is the film density and ΔF is the frequency shift of the QCM. The bulk density of TiO_2-based gel, 1.7 g/cm^3, was used for the calculation of the film thickness.

Preparation of Mg^{2+}-Templated Ultrathin Films. Pure TiO_2 gel films were prepared as a control by the surface sol−gel process. In a typical preparation of Mg^{2+}-templated ultrathin films, 0.0114 g of $Mg(O\text{-}Et)_2$ was dissolved in 10 mL of 2-ethoxyethanol, with the aid of an ultrasonic bath and stirring for 5 days. Ti(O-*n*Bu)$_4$ (0.3531 mL) was then added with stirring, and the mixture was stirred further for 1 h. The composition of the mixed solution was 10 mM $Mg(O\text{-}Et)_2$ and 100 mM Ti(O-*n*Bu)$_4$. A mercaptoethanol-modified electrode was immersed in this solution at room temperature for 10 min and then rinsed with toluene for 1 min to remove the physisorbed species and dried with nitrogen gas. Then, the electrode was attached to a QCM frequency counter and kept in air until the frequency change, probably due to the progress of the hydrolysis of surface alkoxide groups, became insignificant. These steps constitute one cycle of chemisorption and activation.

Removal and Incorporation of Metal Ions and Calcination of Thin Films. To remove the metal ions, the thin film was immersed in aqueous HCl of pH 4 for 10−20 min, rinsed with pure water for 2 min, and dried with nitrogen gas. It was then treated with aqueous NaOH (pH 10) for 10−20 min, followed by rinsing with pure water for 2 min and drying with nitrogen gas. The frequency of the film was measured at this stage. The resonator was then immersed in an aqueous solution of metal ions (0.01−10 mM) for 20 min or 4 h, rinsed with pure water for 30−60 s and dried by being flushed with nitrogen gas. The frequency shift was recorded and used to calculate the mass of incorporated metal ion. Calcination was carried out in a programmable KDF-S70 furnace manufactured by Denken, Kyoto, Japan. The samples were heated at a rate of 22.5 or 25 °C·min^{-1} to 450 or 500 °C and then kept at that temperature for 30 min. The samples were subsequently allowed to cool to room temperature.

X-ray Photoelectron Spectroscopy (XPS) and Scanning Electron Microscopy (SEM). For XPS measurements, the films were assembled on quartz plates that had been cleaned first with concentrated sulfuric acid (96%) and then rinsed in ultrapure water and dried with N_2, followed by a second cleaning with 1 wt % ethanolic KOH solution (ethanol/water = 3:2, v/v). The XPS measurements were carried out on ESCALAB 250 instrument (VG) using Al Kα (1486.6 eV) radiation. The applied power was operated at 15 kV and 20 mA. The base pressure in the analysis chamber was less than 10^{-8} Pa. Smoothing, background removal, and peak fitting were carried out with the VG analysis software package ECLIPS. All of the peaks were corrected with C 1s (285 eV) as the reference. For SEM observations, the films on QCM

(18) Magruder, R. H., III; Zuhr, R. A. *Nucl. Instrum. Meth*ods *Phys. Res. B* **1998**, *141*, 256−260.
(19) Yabe, S.; Yamashita, M.; Suzuki, K.; Momose, S.; Tahira, K.; Yoshida, S.; Li, R.; Yin, S.; Sato, T. In *Proceedings of the 79th CSJ National Meeting*; Chemical Society of Japan: Tokyo, Japan, 2001; p 293.
(20) Dong, D.; Jiang, S.; Men, Y.; Ji, X.; Jiang, B. *Adv. Mater.* **2000**, *12*, 646−649.
(21) Fukumura, T.; Jin, Z. W.; Ohtomo, A.; Koinuma, H.; Kawasaki, M. *Appl. Phys. Lett.* **1999**, *75*, 3366−3368.
(22) Matsumoto, Y.; Murakami, M.; Shono, T.; Hasegawa, T.; Fukumura, T.; Kawasaki, M.; Ahmet, P.; Chikyow, T.; Koshihara, S.; Koinuma, H. *Science* **2001**, *291*, 854−856.
(23) Ichinose, I.; Senzu, H.; Kunitake, T. *Chem. Lett.* **1996**, 831−832.
(24) Lee, S.-W.; Ichinose, I.; Kunitake, T. *Langmuir* **1998**, *14*, 2857−2863.
(25) Lee, S.-W.; Ichinose, I.; Kunitake, T. *Chem. Lett.* **1998**, 1193−1194.
(26) He, J.; Ichinose, I.; Kunitake, T. *Chem. Lett.* **2001**, 850−851.
(27) Sauerbrey, G. *Z. Phys.* **1959**, *155*, 206−222.

Scheme 1. Template Approach to the Incorporation of a Second Metal Ion into TiO_2 Ultrathin Films

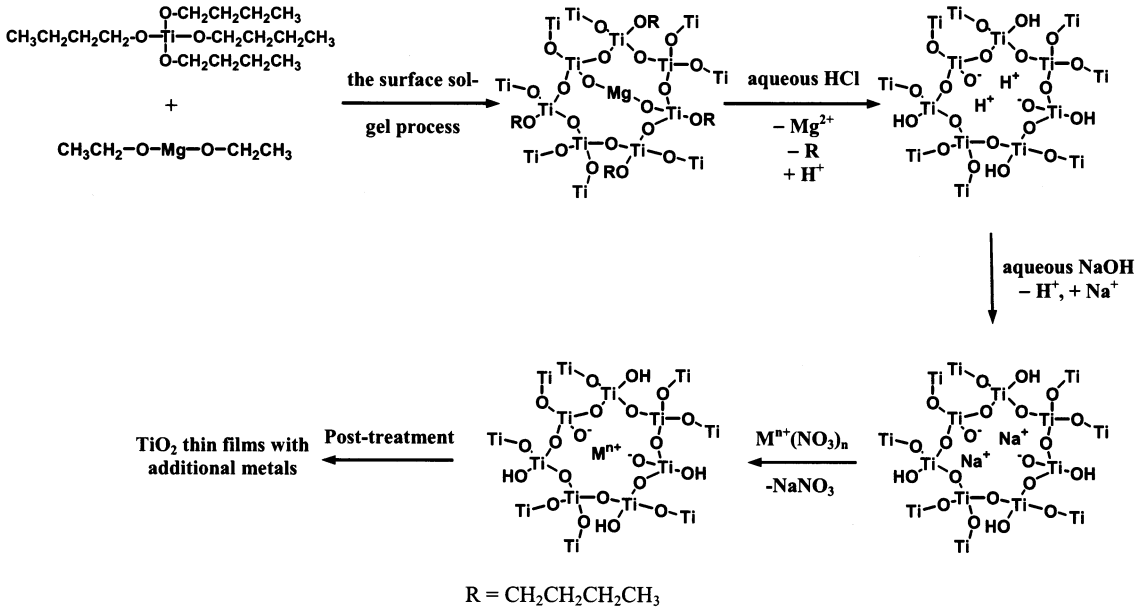

R = $CH_2CH_2CH_2CH_3$

electrodes were cleaved, and 2 nm of Pt was coated on them with a Hitachi E-1030 ion-coater. Then, the films were observed on a Hitachi S-900 scanning electron microscope.

UV−Visible Absorption Spectra and ATR Infrared Spectra. The samples were assembled on quartz plates. Their UV−visible absorption spectra were recorded with a quartz plate as the background on a Shimadzu UV-3100PC UV−vis−NIR scanning spectrophotometer. The attenuated total reflection (ATR) IR spectra were measured with air or a quartz plate as the background on a Nicolet Avatar 320 FT-IR spectrometer with an Omni sampler accessory.

Results and Discussion

Assembly of Thin Films with Ion-Exchange Sites. We adopted a template approach for film assembly, as illustrated in Scheme 1. The template metal alkoxide should meet the following requirements: (1) it readily reacts with Ti(O-*n*Bu)$_4$ to form Ti−O−M linkages rather than separate M−O−M linkages during the surface sol−gel process; (2) it can be selectively removed from TiO_2 matrixes by simple treatments. We tested the following metal alkoxides for this purpose: Sm(O-*i*Pr)$_3$, La(O-*i*Pr)$_3$, Ce(O-*i*Pr)$_3$, Fe(O-Et)$_3$, and Mg(O-Et)$_2$. The first three compounds did not show satisfactory solubilities in common organic solvents, such as tetrahydrofuran, 1,4-dioxane, 1,2-dimethoxyethane, and 2-ethoxyethanol, and we could not obtain suitable precursor solutions. Fe(O-Et)$_3$ showed a good solubility in 2-ethoxyethanol, but Fe^{3+} ion was not readily removed from the TiO_2 matrix. Mg(O-Et)$_2$ is soluble in solvents such as 2-ethoxyethanol, ethanol, and methanol. Also, the Mg^{2+} ion can be removed from mixed TiO_2 thin films. Thus, we chose Mg(O-Et)$_2$ as the template.

A QCM was used to monitor the film growth process for both single-component and mixed TiO_2 gel films. Frequency shifts increase in proportion to adsorption cycles in the absence and presence of Mg(O-Et)$_2$ (Figure 1a and b). The frequency shift per cycle becomes greater at higher Mg(O-Et)$_2$ concentrations (Figure 1c and d), but it deviates from linearity. The thickness of the eight-layer film was estimated to be 20 nm for Figure 1b and 8.5 nm for Figure 1a (see the Experimental Section).

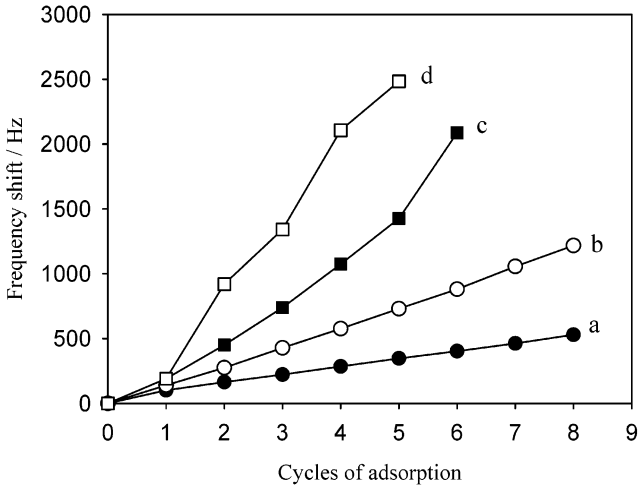

Figure 1. Assembly of TiO_2 gel films in the presence of Mg(O-Et)$_2$ at concentrations of (a) 0, (b) 10, (c) 100, and (d) 300 mM [100 mM Ti(O-*n*Bu)$_4$, 2-ethoxyethanol as the solvent, toluene as the rinsing solvent, room temperature]. The conditions for film assembly in the subsequent figures are the same as those of part b.

The enhanced adsorption in the presence of Mg(O-Et)$_2$ was probably due to the high basicity of the template.

When this film was treated with aqueous HCl (pH 4), a QCM frequency increase of 221 Hz was recorded. This appears to result from the removal of Mg^{2+} and the accompanying hydrolysis of unhydrolyzed alkoxide groups (Scheme 1). Further treatment of this film with aqueous NaOH (pH 10) resulted in a QCM frequency decrease of 80 Hz, apparently due to replacement of protons by sodium ions.

It must be emphasized at this point that the QCM data represent a qualitative measure of the ion-exchange process, and XPS measurements were carried out to confirm the QCM results. The XPS peaks observed for the as-prepared, two-component film are centered at 89 eV (Mg 2s) and 50 eV (Mg 2p) and at 62 eV (Ti 3s), 465 eV (Ti $2p_{1/2}$), 459 eV (Ti $2p_{3/2}$), and 37 eV (Ti 3p) (Figure 2a), indicating that both Mg and Ti

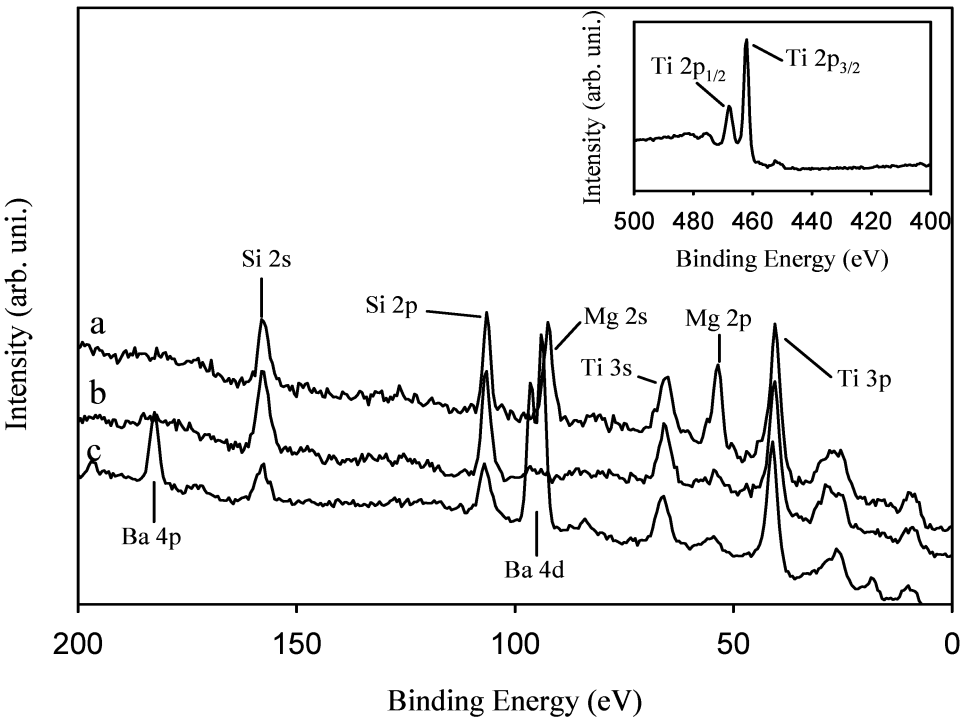

Figure 2. XPS spectra of Mg^{2+}-templated TiO_2 thin films (a) before and (b) after removal of Mg^{2+} and (c) after incorporation of Ba^{2+} ions [10 mM aqueous $Ba(NO_3)_2$, 4-h immersion time]. The inset shows the expanded spectrum between 500 and 400 eV. The three spectra agree exactly.

exist in the TiO_2 thin film. The peak at 155 eV was assigned to Si 2s of the quartz substrate. Peaks below 35 eV were difficult to assign, because they came from valence bands. Treatment of the film with acidic and alkali solutions resulted in the disappearance of the Mg peaks (Figure 2b). In contrast, the intensities of the Ti peaks remained unchanged, indicating that the TiO_2 gel was stable under the treatment conditions. This is in agreement with our independent tests on pure TiO_2 gel films, which showed that TiO_2 gel films do not deteriorate in solution in the pH range of 3.0−13.3.[28] Thus, stable TiO_2 gel films with ion-exchange sites were formed, as illustrated in Scheme 1.

Incorporation of Metal Ions by Ion Exchange. The Mg^{2+}-templated film was then subjected to doping with a variety of metal ions by immersion in aqueous solutions of metal ion nitrates. The mass increase upon 20 min of immersion for a templated film of 51-nm thickness was estimated from the frequency decrease. This mass increase is an overall change that includes accompanying reactions and structural modifications of the film in addition to the incorporation of metal ion. Thus, it does not represent the exact amount of metal ion introduced. In spite of these shortcomings, the QCM frequency change is highly useful as a qualitative measure of metal ion incorporation. The general trend of incorporation, as expressed simply by the mass increase divided by the atomic mass of the corresponding metal, is shown in Figure 3. The QCM mass increase is enhanced in the order Li^+, K^+ < Mg^{2+}, Ca^{2+}, Ba^{2+} < La^{3+}, Gd^{3+}, and it appears that the charge number is

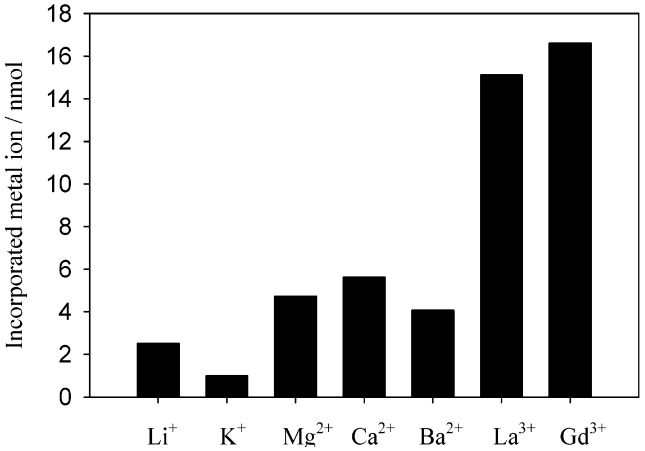

Figure 3. Incorporation of various metal ions into Mg^{2+}-templated TiO_2 thin films (51 nm), as estimated from QCM frequency changes divided by atomic mass (10 mM aqueous metal ion nitrate, 20-min immersion time, room temperature).

reflected in the extent of incorporation. However, this result is not necessarily consistent with the XPS data of Table 1. Therefore, a quantitative discussion is made with the latter data.

As discussed above, after removal of template Mg^{2+} species, ion-exchange sites are created in thin films. The validity of the ion-exchange mechanism was further supported by SEM observations, as well as ATR IR and XPS measurements. For example, doping of Ba^{2+} for 4, 10, 25, and 50 h did not result in any crystal growth of metal salt on the film surface (SEM observations), unlike single-component TiO_2 films where metal salts tended to crystallize on their smooth surfaces. After removal of the template Mg^{2+} ions, nanopores (less than 2 nm, TEM observtions) were formed in the film, preventing the deposition of metal salts by crystalliza-

(28) The stability of TiO_2 gel films was tested in environments of varying pH by using aqueous HCl and NaOH. In the range of $3.0 \leq pH \leq 13.3$, the gel film was stable. At pH 2 or 13.7, the gel film was partially damaged. At pH 1 (0.1 M HCl) or pH 14 (1 M NaOH) and above, the gel film was totally destroyed.

Table 1. Atomic Ratios of Doped Metal Ions to Ti As Determined by XPS Peak Intensities[a,b]

M	M/Ti	M/Mg	binding energy (eV)	assignment	M	M/Ti	M/Mg	binding energy (eV)	assignment	M	M/Ti	M/Mg	binding energy (eV)	assignment
Ba	1.4	1.2	781	$3d_{5/2}$	Fe	2.2	1.9	711	$2p_{3/2}$	Ag	3.6	3.1	369	$3d_{5/2}$
Cr	0.20	0.17	578	$2p_{3/2}$	Co	1.2	1.0	781	$2p_{3/2}$	Cd	0.33	0.28	406	$3d_{5/2}$
Mn	0.26	0.22	642	$2p_{3/2}$	Pd	0.14	0.12	337	$3d_{5/2}$	Gd	0.3−0.7	0.3−0.7	143	4d

[a] The concentration of aqueous metal ion nitrate was 10 mM, and the immersion time was 4 h. [b] The Mg/Ti ratio in the as-prepared thin film was 1.2.

tion. IR peaks (1390, 830, 720 cm^{-1}) and the XPS peak (407 eV) characteristic of NO_3^- were not found, indicating that metal ions alone were incorporated into the matrix network without the adsorption of metal nitrates themselves. All of these results clearly show an ion-exchange mechanism for the approach described herein.

The generality of metal ion incorporation was additionally confirmed by XPS measurements of the doped films on quartz plates (Figure 2 and Table 1). In the as-prepared film, the Mg/Ti ratio was estimated to be 1.2 from the XPS peak areas. All of the tested metal ions representative of main group, transition, and lanthanide metal ions were successfully incorporated into the TiO_2 matrixes. The amounts of metal ions introduced (M/Ti ratios) varied greatly under identical conditions. From the M/Ti and Mg/Ti values, the number of metal ions incorporated per ion-exchange site was estimated and is expressed as M/Mg in Table 1. The Gd^{3+} peak overlaps partially with the Si peak, making it difficult to obtain accurate data. Thus, the Gd^{3+}M/Ti and Gd^{3+}M/Mg ratios were estimated to be in the range of 0.3−0.7. Pd^{2+}, Mn^{2+}, Cd^{2+}, and Cr^{3+} fall in the ranges of M/Ti = 0.1−0.4 and M/Mg = 0.1−0.3, indicating that the ion-exchange sites are not fully occupied by these metal ions. Co^{2+} and Ba^{2+} have M/Ti values of 1−1.5 and M/Mg values of ca. 1, showing essentially stoichiometric ion exchange. In the case of Fe^{3+}, the M/Ti and M/Mg ratios reach 2.2 and 1.9, respectively, three times as large as the charge-based exchange. It is known that Fe^{3+} can form ol complexes in aqueous solutions. The high ratios might originate from the olation effect. Ag^+ also gives a much larger doping efficiency than other monovalent metal ions (Li^+, K^+). This might be caused by the photoreduction of Ag^+ ions.

The Nature of the Ion-Exchange Process. An important feature of the current approach is that incorporated metal ions could be quantitatively removed and reloaded under mild conditions for at least several cycles with limited deterioration of the ion-exchange capacity. It is clear that both the film matrix and the ion-exchange site are stable and robust. This reversible process, on one hand, allows for many trial adsorptions to be executed on a single thin film, providing an efficient tool for examining the adsorption process. On the other hand, such a matrix itself might be used for the separation and recovery of metal ions for which the reversible process is essential.

The reversible ion exchange is naturally dependent on the reaction time and reactant concentration. As shown in Figure 4, the amount of Gd^{3+} ions incorporated into thin film increases rapidly in the early stages and less rapidly in the later stages. Ion incorporation appears to saturate in 10−12 h. The effect of the Gd^{3+} concentration on ion exchange was studied for an immersion time of 20 min, where a gradual increase in

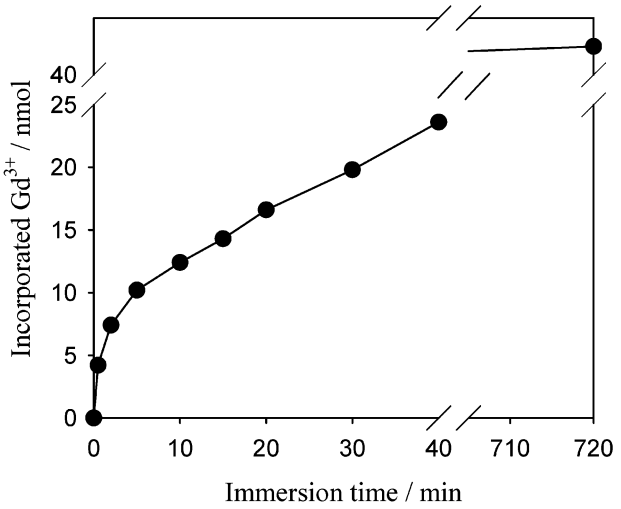

Figure 4. QCM dependence of the quantity of incorporated Gd^{3+} ions on immersion time [10 mM aqueous $Gd(NO_3)_3$, room temperature].

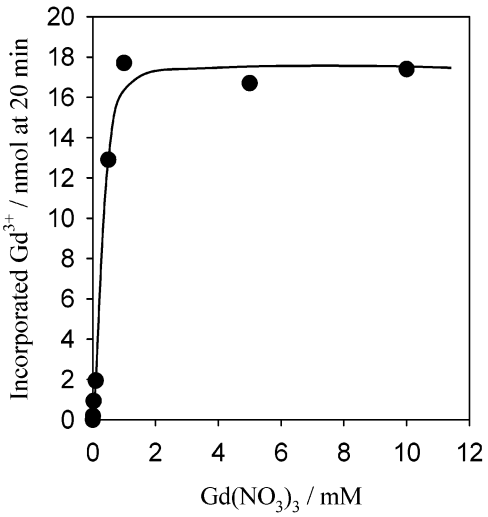

Figure 5. QCM dependence of the quantity of incorporated Gd^{3+} ions on the Gd^{3+} concentration in the immersion solution (20-min immersion time, room temperature).

Gd^{3+} incorporation is observed. Figure 5 illustrates that the Gd^{3+} incorporation increases sharply in the concentration range of 0−1 mM $Gd(NO_3)_3$. However, it is constant in the higher concentration range we examined, indicating that the exchange rate is zeroth order in the Gd^{3+} concentration. Note that the Gd^{3+} incorporation increases linearly with time under these experimental conditions (Figure 4). It is clear that the overall rate of the ion exchange is governed by several kinetic processes. The ion-exchange process might consist of five steps as represented in Scheme 2: (1) diffusion of Gd^{3+} from the solution to the film surface, (2) diffusion of Gd^{3+} inside the film, (3) ion-exchange reaction (Gd^{3+} +

Scheme 2. Schematic Representation of the Ion-Exchange Process[a]

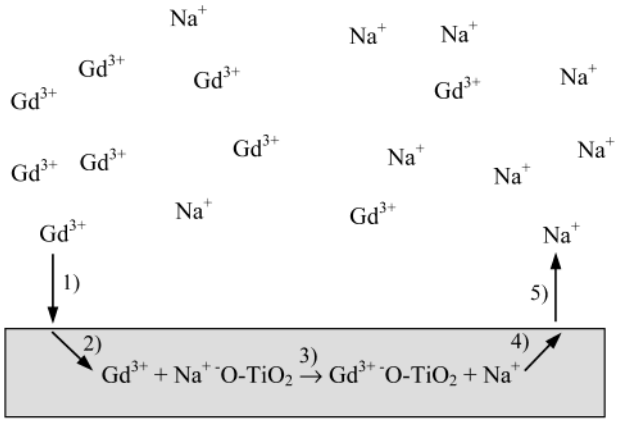

[a] Counterion NO_3^- not shown here for simplicity.

$Na-O-TiO_2 \rightarrow Gd-O-TiO_2 + Na^+$), (4) diffusion of Na^+ to the film surface, and (5) diffusion of Na^+ away from the film surface into the solution. Process 1 would be rate-determining at very low Gd^{3+} concentrations, as evidenced by a rapid rise in Figure 5. At higher Gd^{3+} concentrations in bulk solution, process 1 is no longer rate-determining. In this region, ion exchange proceeds according to zeroth-order kinetics, suggesting that the later processes (processes 2−4) are rate-determining. Process 5 cannot be rate-determining, because the Na^+ concentration in solution is extremely small. The diffusive migration of Gd^{3+} and Na^+ ions within the film (processes 2 and 4) can not be rate-determining, if we consider the ultrathin nature and loose gel structure of the film matrix. Then, the ion-exchange step itself appears to be rate-limiting, although further investigations are needed to clarify this point.

Calcination of Metal-Ion-Doped Thin Films. Metal ions introduced by ion exchange are labile and can be readily removed under acidic conditions. Complete immobilization of these metal ions in TiO_2 matrixes is achieved by calcination. Calcination was carried out at 450 °C for 30 min. Figure 6 shows ATR IR spectra of a Mg^{2+}-templated thin film (Mg^{2+} removed) and of a Ba^{2+}-doped thin film before and after calcination. In Figure 6a, peaks at 2956, 2925, and 2854 cm^{-1} (C−H stretching vibrations) indicate the existence of unhydrolyzed alkoxide groups (Ti−O−*n*Bu) after Mg^{2+} removal. The broad peak around 3400 cm^{-1} is assigned to OH groups of the TiO_2 matrix. After Ba^{2+} doping (Figure 6b), however, the C−H peaks decreased sharply, probably as a result of hydrolysis of the remaining alkoxide groups during doping. Further calcination resulted in complete disappearance of the C−H peaks and the broad O−H peak (Figure 6c).

The effect of calcination on film morphology was studied by SEM for these three films. These films appear flat, smooth, and transparent macroscopically. On the microscopic scale, some gel particles can be seen scattered on the film surface (Figure 7a).[29] Doping of Ba^{2+} did not result in morphology changes (SEM image not shown). Significant morphology changes were also not observed for the calcined Ba^{2+}-doped film (Figure 7b). As shown in Table 1, the templated film could efficiently incorporate Ba^{2+} ions to give ratios of Ba/Ti = 1.4 and $Ba/Mg_{template} = 1.2$ at an immersion time of 4 h in 10 mM aqueous $Ba(NO_3)_2$. In contrast, when the templated film was calcined before doping, subsequent immersion of this film in aqueous $Ba(NO_3)_2$ under the same conditions led to only limited Ba^{2+} incorporation (Ba/Ti = 0.14 and $Ba/Mg_{template} = 0.12$). Apparently, the ion-exchange sites (Na^+ sites) were inactivated by calcination.

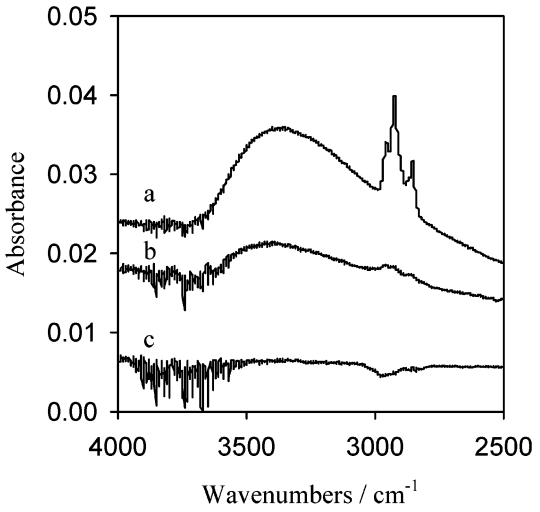

Figure 6. ATR IR spectra of (a) templated (Mg^{2+} removed), (b) Ba^{2+}-doped, and (c) calcined Ba^{2+}-doped TiO_2 ultrathin films. Doping conditions: 10 mM aqueous $Ba(NO_3)_2$, 4-h doping time, room temperature.

It can be concluded from the preceding IR, SEM, and XPS results that the organic moeties and trapped water molecules were burned or driven out during calcination and that the existing hydroxy groups further cross-linked to form Ti−O−Ti linkages, resulting in a much tighter gel network. Lack of the nanoporous structure might lead to the low ion-exchange ability after calcination.

Elongation of UV Absorption Edge of Doped TiO_2 Films. A primary interest of metal ion doping is to enhance the optical absorption of the TiO_2 matrix in the near-UV and visible regions, to improve the photocatalytic and photoelectrochemical activities. This has been achieved, for example, by MOCVD,[1d] ion impregnation,[5] and ion implantation.[30] UV−visible spectra of undoped thin films are shown in Figure 8A. The as-prepared TiO_2/MgO film shows the shortest onset wavelength at 316 nm. After removal of Mg^{2+}, the absorption spectrum is red-shifted and has an onset wavelength at 325 nm. Anpo and co-workers reported that UV−visible reflectance spectra were blue-shifted when the fraction of TiO_2 was decreased in TiO_2/SiO_2 binary oxide catalysts.[4] In contrast, the calcination in our case leads to a small red shift with an onset wavelength at 331 nm. This onset wavelength is considerably blue-shifted from that of bulk TiO_2 (anatase, 387 nm; rutile, 413 nm) as well as those of the quantum-size TiO_2 (370 nm for 24-Å anatase, 375.1 nm for 38-Å anatase, and 398 nm for 55-Å rutile). It appears that this film is composed of very fine condensates of TiO_2.[31]

(29) Ichinose, I.; Senzu, H.; Kunitake, T. *Chem. Mater.* **1997**, *9*, 1296−1298.

(30) Ichihashi, Y.; Yamashita, H.; Anpo, M. *Funct. Mater.* **1996**, *16*, 12.

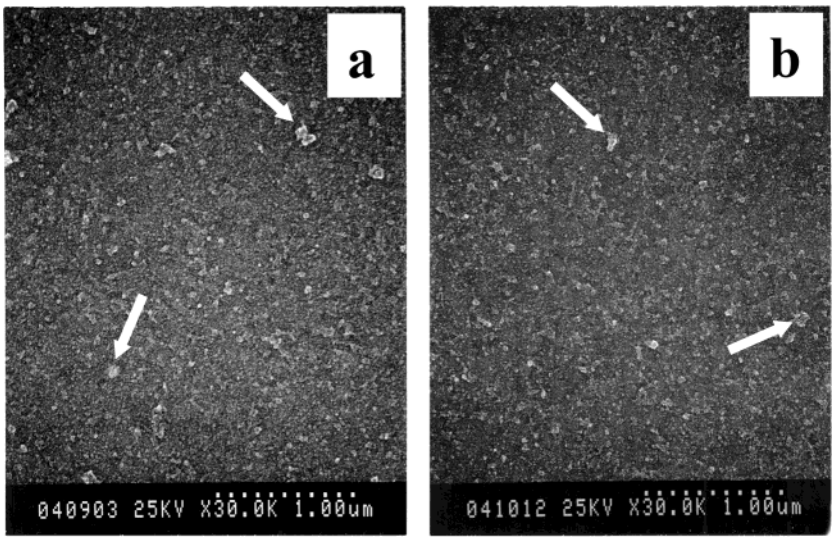

Figure 7. SEM images of (a) templated (Mg^{2+} removed) and (b) calcined Ba^{2+}-doped TiO_2 ultrathin films. The samples are identical to those in parts a and c of Figure 6, respectively. The arrows point to gel particles.

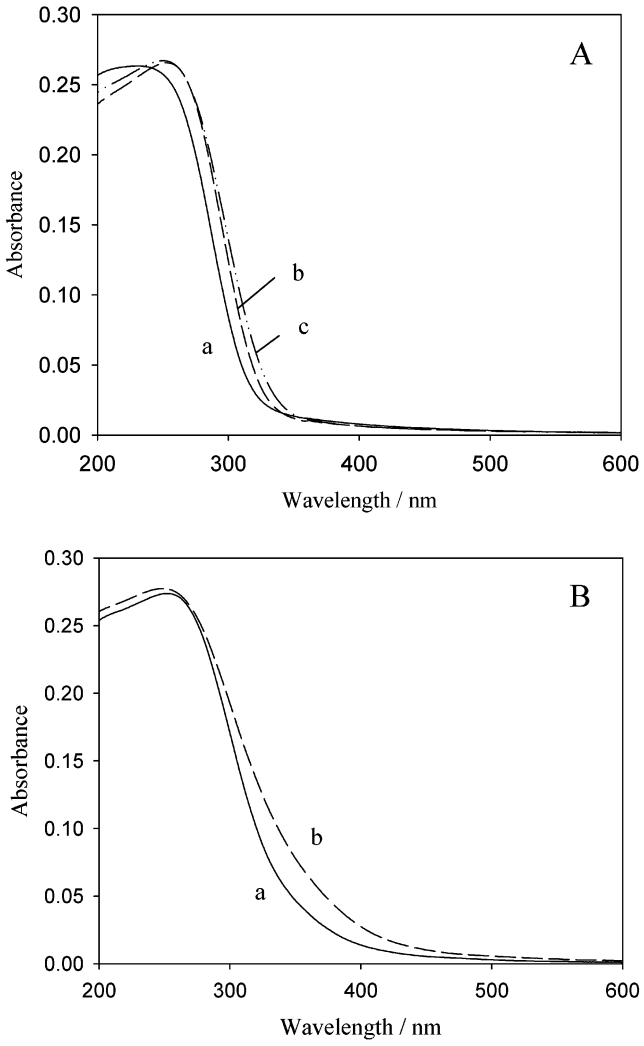

Figure 8. (A) UV−visible spectra of (a) MgO/TiO_2, (b) templated (Mg^{2+} removed), and (c) calcined TiO_2 ultrathin films. (B) UV−visible spectra of (a) Fe^{3+}-doped and (b) calcined Fe^{3+}-doped TiO_2 ultrathin films. Doping conditions: 10 mM aqueous $Fe(NO_3)_3$, 4-h doping time, room temperature.

When Cr^{3+} and Fe^{3+} are introduced into TiO_2 networks (without calcination), the absorption spectra are red-shifted by 7 and 22 nm, respectively (Figure 8B and Table 2). When calcined, a Cr^{3+}-doped film shows a red shift of 11 nm, and an Fe^{3+}-doped film exhibits a red shift of 82 nm for the onset wavelength relative to that of the calcined but undoped film. In fact, the absorption edge is extended into the visible region. Iron doping by impregnation[5] or MOCVD[1d] was reported to have remarkable effects on the photocatalytic and photoelectrochemical properties of TiO_2. A high quantum efficiency was observed even at long wavelengths. The current doping method provides a novel, efficient approach for the preparation of such materials.

Table 2. UV−Visible Spectra of Ultrathin Films[a]

ultrathin films	onset wavelength (nm)	
	Cr^{3+}-doped	Fe^{3+}-doped
as-prepared TiO_2/MgO film	316	316
Mg^{2+}-templated film (Mg^{2+} removed)	325	325
calcined Mg^{2+}-templated film	331	331
metal-ion-doped film	332	347
calcined metal-ion-doped film	342	413

[a] The doping conditions were the same as those in Table 1.

Conclusion

In the present study, we developed a novel template approach for the incorporation of a variety of second metal ions in ultrathin TiO_2 films. The Mg^{2+} template was very efficient for creating the ion-exchange site. There are conceivably two major implications for the current results. First, it is the formation of robust ion-exchange sites during the surface sol−gel preparation of TiO_2 matrixes. A stable network topology that corresponds to the ion-exchange site is preserved in the TiO_2 matrix. We showed previously that structural characteristics of organic molecules are imprinted in the TiO_2 gel.[24] The effectiveness of the Mg^{2+} template suggests the same conclusion.

Second, ion exchange can lead to many novel functional materials. As described in the Introduction, the doping of second metal ions into metal oxide matrixes

(31) Moriguchi, I.; Maeda, H.; Teraoka, Y.; Kagawa, S. *J. Am. Chem. Soc.* **1995**, *117*, 1139−1140.

is an important method of exploring functional materials. Our method is facile and general. The incorporated metal ions are readily immobilized by calcination. These features should be highly advantageous in designing catalytic, electronic, optoelectronic, and magnetic properties in metal oxide films. For example, we have succeeded in the size-controlled preparation of nanoparticles (single-component, alloy, and core−shell types) of various metal elements by using the above ion-exchange approach and will publish the results in a future report.

Acknowledgment. J. He is grateful to the Japan Science and Technology Corporation (JST) for a STA fellowship.

CM010880W